Extended Si {311} defects

Jeongnim Kim* and John W. Wilkins

Department of Physics, The Ohio State University, Columbus, Ohio 43210

Furrukh S. Khan

Department of Electrical Engineering, The Ohio State University, Columbus, Ohio 43210

Andrew Canning

Cray Research Swizerland, PSE, EPFL, Lausanne, Switzerland
(Received 15 August 1996; revised manuscript received 6 November 1996)

We perform total-energy calculations based on the tight-binding Hamiltonian scheme (i) to study the structural properties and energetics of the extended {311} defects depending upon their dimensions and interstitial concentrations and (ii) to find possible mechanisms of interstitial capture by and release from the {311} defects. The generalized orbital-based linear-scaling method implemented on the Cray T3D is used for supercell calculations of large-scale systems containing more than 1000 Si atoms. We investigate the {311} defects systematically from few-interstitial clusters to planar defects. For a given defect configuration, constant-temperature molecular-dynamics simulations are performed at 300–600 K for about 1 psec to avoid trapping in the local minima of the atomic structures with small energy barriers. We find that interstitial chain structures along the $\langle 011 \rangle$ direction are stable interstitial defects with respect to isolated interstitials. The interstitial chains provide basic building blocks of the extended {311} defects, i.e., the extended {311} defects are formed by condensation of the interstitial chains side by side in the $\langle 233 \rangle$ direction. We find that successive rotations of pairs of atoms in the {011} plane are mechanisms with a relatively small energy barrier for propagation of interstitial chains. These mechanisms, together with the interstitial chain structure, can explain the growth of the {311} defects and related structures such as V-shape bend structures and atomic steps observed in transmission electron microscopy images. [S0163-1829(97)03123-8]

I. INTRODUCTION

The decreasing size of semiconductor devices requires precise control of device structures, particularly dopant distributions. Ion implantation introduces energetic charged atomic particles in a substrate for the purpose of changing electrical, metallurgical, and chemical properties of the substrate. The wide use of ion implantation is due to its precise control over total dopant doses, depth profiles, and the area uniformity. However, ion implantation induces transient enhanced diffusion (TED) of dopants: The diffusivity of the dopants is abnormally enhanced for a transient period of time after ion implantation.[1] Many studies have suggested that lattice damages, introduced during ion implantation, are responsible for fast diffusion of dopants.[2,3]

In particular, the diffusivity of boron during annealing in ion-implanted samples is enhanced by many orders of magnitude greater than B diffusivity in a thermal equilibrium.[2] This transient enhanced diffusion of B places limitations of the use of B^+ implantation in fabricating submicron devices. Boron TED occurs due to excessive Si interstitials, which are created by B^+ implantation and contribute to the fast diffusion of B.[1,3] The boron diffusion via pairing of B and Si interstitials has been supported by experiments and theories.[1] Experiments observe enhancement of the B diffusivity when Si interstitials are selectively injected by surface oxidation[4] and by Si^+ implantation.[3] First-principle calculations reported that the activation energy of B diffusion associated with Si interstitials is the lowest among possible diffusion

mechanisms.[5,6] Therefore, the concentration of Si interstitials after the ion implantation and during the thermal annealing process is an important parameter to determine the final depth profile of B in the ion-implanted samples.

The concentration of Si interstitials depends on (i) the ion implantation conditions, i.e., the incident energy and the dose, and (ii) the temperature at which thermal annealing is performed. Implantation at a higher incident energy or with a higher dose of the ions generates more Si interstitials. As the name transient enhanced diffusion indicates, the enhancement factor of the B diffusivity decays as the thermal annealing proceeds, and eventually the diffusivity of the B converges to that in a thermal equilibrium. The temporal extent of the enhanced diffusion of B decrease at higher annealing temperatures since the excessive Si interstitials migrate to the regular lattice sites in a shorter period of time.[2] It is observed that the temporal extent (duration of the boron TED) is exponentially activated. The activation energy, depending on the ion implantation conditions, shows a large variance: 1–5 eV.[7,8]

This activation energy summarizes complex processes for B diffusion in ion-implanted samples: generation, diffusion, and annihilation of the Si interstitials as well as the interactions of B with the B and Si interstitials. Recently, Eaglesham *et al.*[9] and Stolk *et al.*[10] suggested that emission of Si interstitials from particular extended defects, namely, {311} defects, causes the boron TED. They observed that the dissolution of the {311} defects occurs at the same time and the temperature conditions as boron TED. The extended {311}

defects are detected under B^+ implantation at an incident energy of few tens of keV (Refs. 3 and 10) and the corresponding activation energy of the boron TED was obtained at 3–5 eV.[7] The high value of the activation energy can be related to the stability of the {311} defects with respect to isolated interstitials. However, boron TED has been also observed without detecting any macroscopic defect, when the energy of the B^+ implantation decreases below 10 keV.[8] A lower activation energy (about 1 eV) was estimated for this low-energy ion implantation. This low-energy B^+-implantation experiment suggests that the formation of stable {311} defects depends on the interstitial concentrations. Furthermore, the observation of boron TED in the absence of the observable {311} defects suggests that microscopic interstitial clusters may exist and contribute to the B diffusion by releasing interstitials at a lower energy cost. It is possible that the microscopic interstitial clusters are related to the {311} defects and the formation and dissolution of the defects, from the interstitial clusters to the extended {311} defects, can be explained by common mechanisms.

The proposition that the {311} defects are formed by condensation of interstitials and provide interstitial sources during boron TED has been supported by experiments using a variety of procedures to inject Si interstitials into bulk systems: The {311} defects are observed to be formed by surface oxidation,[4] by GeV-electron irradiation,[11] and by ion implantations.[10]

The {311} defects are often called *rodlike* because they are typically elongated along the $\langle 011 \rangle$ direction as much as 1 μm.[11,12] The width of the {311} defects ranges 1–100 nm along the $\langle 233 \rangle$ direction, perpendicular to the elongation direction. The name {311} defects indicates the observed habit plane[13] on which the rodlike defects lie, namely, the {311} plane formed by the $\langle 011 \rangle$ and $\langle 233 \rangle$ directions.

Here we present total-energy calculations based on the tight-binding Hamiltonian scheme (i) to study the structural properties and energetics of the {311} defects as a function of their dimensions and interstitial concentrations and (ii) to find possible mechanisms of interstitial capture by and release from the {311} defects. We investigate the {311} defects systematically from few-interstitial clusters to planar defects. Our results can be summarized as follows.

(i) *Interstitial chain: The basic building block of the {311} defects.* We show that an interstitial chain along the $\langle 011 \rangle$ direction is stable with respect to isolated interstitials. The formation energy of the interstitial chains, $E_{int}^f = 2$ eV per interstitial, is smaller than the formation energies of isolated interstitials, 3–5 eV. Interstitial chains constitute basic building blocks of the {311} defects, i.e., extended defects on the {311} habit plane can be constructed by arranging the interstitial chains along the $\langle 233 \rangle$ direction (Secs. III and IV A).

(ii) *Stability of the {311} defects.* Interstitial chains along the $\langle 011 \rangle$ direction are stable against the isolated interstitials if they contain more than two interstitials. The formation energy per interstitial decreases linearly with the length of the interstitial chains along the $\langle 011 \rangle$ directions. More stable extended {311} defects than isolated interstitial chains are formed by condensation of interstitial chains along the $\langle 233 \rangle$ direction. The interstitial concentration of the most

stable {311} defect, a planar defect, is 5×10^{14}/cm^2 (Secs. III, IV B, and VII).

(iii) *Growth mechanism.* The stability dependence of the {311} defects on the interstitial concentration indicates that finite-size interstitial clusters capture interstitials to grow into the interstitials chains along the $\langle 011 \rangle$ direction. The elongated interstitial chains are then further stabilized by capturing interstitials or interstitial chains side by side along the $\langle 233 \rangle$ direction. This growth mechanism based on the stability study is in good agreement with the experimental claims that the elongation of the rodlike {311} defects along the $\langle 011 \rangle$ direction precedes the growth in the width along the $\langle 233 \rangle$ direction (Sec. IV B).

(iv) *Propagation of the interstitial chains.* We propose a mechanism that can account for the motion of interstitial chains in the direction perpendicular to the chain direction with a relatively small energy barrier. Successive rotations of pair atoms on the {011} plane displace the interstitial chains. The growth of the {311} defects along the $\langle 233 \rangle$ direction can be explained by propagations of interstitial chains that are attracted to and captured by the already existing {311} defects. We show that V-shaped bend structure and atomic steps found in the transmission electron microscopy (TED) images can be formed by combinations of the interstitial chains and the planar rotations (Secs. V and VI).

II. CALCULATIONAL DETAILS

We perform total-energy calculations based on a linear-scaling method in a tight-binding representation,[14] using supercell methods at the Γ point. A tight-binding (TB) Hamiltonian developed by Kwon *et al.*[15] is used to study the defect structures. This TB Hamiltonian gives a good description of the relative energies and equilibrium volumes of the diamond structure and the metallic phases. One flaw of this Hamiltonian is that its ground-state structure of the crystalline silicon is the clathrate structure, which has the same coordination of the diamond structure and consists of five- and six-member rings.[16] We find the calculated cohesive energy of the clathrate structure is indeed 0.07 eV lower than that of the diamond structure. In addition, the optical phonon frequencies of the diamond structure are overestimated by 30% compared to the experimental values. However, this TB Hamiltonian describes the elastic properties of the diamond structure with an error less than 5% compared to experiments and gives the formation energies of the point defects such as vacancies and interstitials, which are in good agreement with those by the local-density approximation (LDA) calculations.[17–21] The validity and accuracy of this TB Hamiltonian to describe the diamond structure has been addressed by several calculations which show good agreement with the LDA calculations: reconstructions of the Si(100) surface[22] and the 90° partial dislocations in Si (Ref. 24) and hydrogenated amorphous Si.[24]

The total-energy calculations of defects requires large supercells to obtain converged formation energies, mainly due to the long-range structural relaxation. We use the orbital-based linear-scaling method implemented on the Cray T3D.[25] We choose a spherical localization of 6 Å for less than 1% error in the total energy (about 30 meV per atom) compared to those obtained by exact calculations by
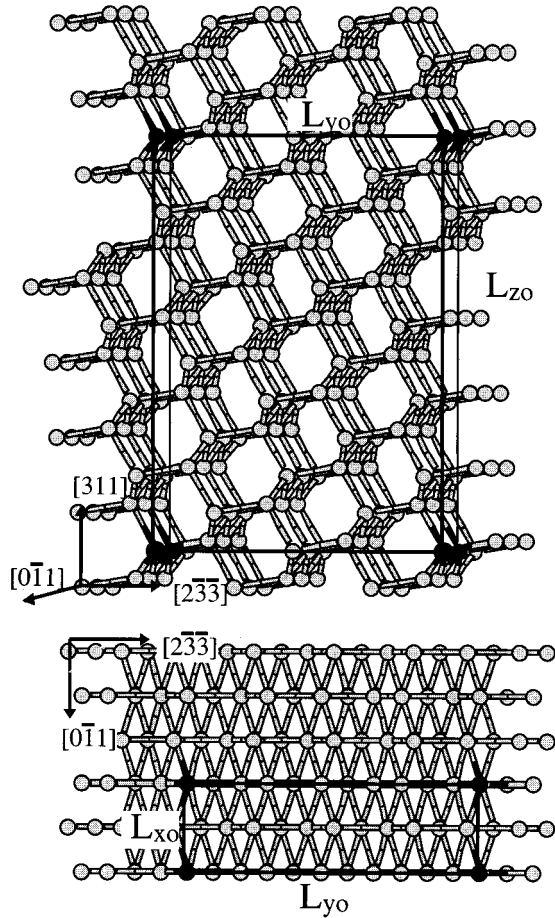
FIG. 1. $\{311\}$ defects. The three principal axes are along the $[0\bar{1}1]$, $[2\bar{3}\bar{3}]$, and $[311]$ directions. For the Si lattice constant ($a=5.43$ Å), the dimensions of the unit cell are $L_{x0}=a/\sqrt{2}$, $L_{y0}=a\sqrt{11}/\sqrt{2}$, and $L_{z0}=a\sqrt{11}$. Supercell calculations at the Γ point are performed by taking a computational cell whose size is $L_x=n_x\times L_{x0}$, $L_y=n_y\times L_{y0}$, and $L_z=2\times L_{z0}$. Periodic boundary conditions are applied in all three directions.

diagonalizations. The chemical potential μ is adjusted to achieve the correct number of electrons with an error less than 10^{-5} electron charge. Significant charge transfer is prevented by using a finite Hubbard-like term ($U=4$ eV); however, few differences are observed from a finite U and $U=0$ in the relaxed atomic structures and in the total energies.

Figure 1 shows the smallest orthorombic unit cell used to study $\{311\}$ defects. The $[311]$ direction, normal to the habit plane of the defects, is chosen as the **z** axis and the $[0\bar{1}1]$ and $[2\bar{3}\bar{3}]$ directions as the **x** and **y** axes, respectively. The unit lengths along the three principal axes are $L_{x0}=a/\sqrt{2}$, $L_{y0}=a\sqrt{11}/\sqrt{2}$, and $L_{z0}=a\sqrt{11}$ for the lattice constant a of the diamond structure Si. The lengths of a computational cell along the $[0\bar{1}1]$ and $[2\bar{3}\bar{3}]$ directions are varied by choosing integer multiples (n_x,n_y) of L_{x0} and L_{y0} and the length along the $[311]$ direction at $L_z=2L_{z0}$. Values for n_x and n_y are chosen so that the displacement of the atoms far from the defect core is less than 0.02 Å with respect to the regular lattice sites of the perfect diamond structure. Periodic boundary conditions are applied along all three directions. For the structural optimizations, initial configurations of the model

structures are given properly and constant-temperature molecular-dynamics (MD) simulations are performed at 300–600 K for about 1 psec to avoid trapping in the local minima of the atomic structures with small energy barriers. Then atomic positions are fully relaxed by using the steepest-descent method until the atomic force on each atom is less than 0.01 eV/Å. The effective temperature of the relaxed ionic configuration is less than 0.1 K.

We define the formation energy of a defect structure that contains N_{int} interstitials and N_{bulk} Si atoms in a computational cell as

$$E^f=E_{tot}[N_{int}+N_{bulk}]-\frac{N_{int}+N_{bulk}}{N_{bulk}}E_{tot}[N_{bulk}].\quad(1)$$

The formation energy per interstitial $E_{int}^f=E^f/N_{int}$ is used to compare defects at a wide range of interstitial concentrations. A smaller E_{int}^f corresponds to a more stable interstitial defect. Calculations using the LDA (Refs. 17–20) and using the TB Hamiltonian[15] found that the $\langle110\rangle$ interstitialcy is the most stable point defect with a formation energy of $3.2-3.9$ eV. Our total-energy calculation using a 1000-Si supercell gives $E_{\langle110\rangle}^f=3.9$ eV.

A binding energy of interstitials with respect to isolated interstitials is defined as

$$-E^b=E^f-N_{int}E_{\langle110\rangle}^f\quad(2)$$

for $E_{\langle110\rangle}^f$, the formation energy of an isolated $\langle110\rangle$ interstitialcy. A positive binding energy of a defect containing interstitials indicates that the interstitial defect is stable with respect to isolated interstitials.

III. INTERSTITIAL CHAINS ALONG THE $\langle011\rangle$ DIRECTION

Here we discuss an interstitial chain structure that is stable against isolated interstitials and constitutes a building block of the $\{311\}$ defects. The interstitial chain structure in Fig. 2 shows that interstitial chains along the $\langle011\rangle$ direction can be inserted into bulk Si without introducing any dangling bond by stacking pair interstitials with a periodicity of L_{x0}. This arrangement of interstitials along the $\langle011\rangle$ direction is favorable since only two dangling bonds would be required for any finite-length interstitial chain.[4,26] Since the number of dangling bonds per interstitial is inversely proportional to the length of the chain, the interstitial chain becomes more stable as it grows along the $\langle011\rangle$ direction. The interstitial chain structures have also been used for an atomic model of planar $\{311\}$ defects by Takeda et al.[27–30]

The most simple defect configuration containing interstitial chains, the structure in Fig. 2(a), is obtained by inserting an interstitial chain into bulk Si. By adding two interstitials per plane, two bonds (dotted line) are broken and two seven-member rings are introduced along the $\pm[311]$ directions. The six-member ring at the center turns into two adjacent five-member rings. The bond-angle distortion ranges from $-23°$ to 20° and the bond-length distortion from -0.13 to 0.03 Å. This chain configuration is a stable interstitial complex with a relatively small formation energy per interstitial, $E_{int}^f=2.2$ eV, compared to that of isolated interstitials (3–5 eV).
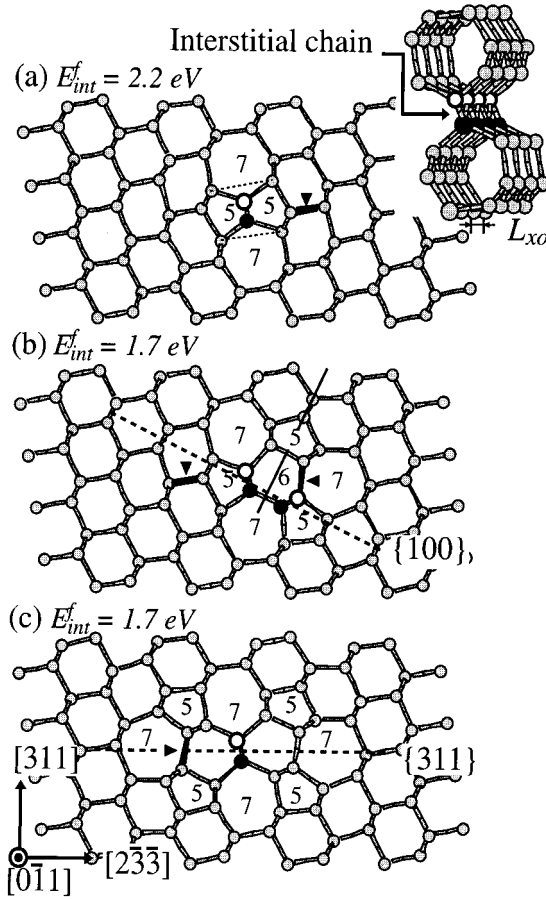
FIG. 2. Interstitial chain obtained by stacking pair interstitials with a periodicity of L_{x0} along the $\langle 011 \rangle$ direction. The solid atoms are $L_{x0}/2$ into the plane with respect to the open-circled atoms. (a) An interstitial chain inserted into bulk Si is surrounded by two adjacent five-member rings. The dotted lines denote the bonds that are broken by the addition of interstitial chains. This structure has a formation energy of 2.2 eV per interstitial. (b) By a rotation of atoms connected by a solid bond (arrow), a more stable structure with $E_{int}^{f} = 1.7$ eV is obtained. The structure has a mirror symmetry with respect to the center of the six-member ring. The dashed line indicates the {100} plane normal to the center line. (c) A rotation of the other bond results in an interstitial chain configuration of $E_{int}^{f} = 1.7$ eV. The symmetry of the structure is an inversion symmetry with respect to the center of pair interstitials on the {311} plane (dashed line).

More stable structures can be obtained by eliminating five-member rings that share common bonds. A rotation of the atoms, connected by a solid bond indicated by an arrow, converts the right five-member ring in Fig. 2(a) into a six-member ring in Fig. 2(b) and lowers the formation energy to 1.7 eV. This defect structure is characterized by a six-member ring surrounded by five- and seven-member rings and has a mirror symmetry with respect to the center of the six-member ring.[31] While the concentration of the additional atoms is two per unit length (L_{x0}), this configuration appears to have two interstitial chains due to its symmetry.

A rotation of the other solid bond results in an interstitial chain surrounded by six- and five-member rings in Fig. 2(c). This configuration has an inversion symmetry with respect to the center of the interstitial pairs. The formation energy is

TABLE I. Formation energy per interstitial, E_{int}^{f} in Eq. (1), and the binding energy, E^{b} in Eq. (2), of few-interstitial clusters. The interstitial clusters are constructed by inserting interstitial chains between bulk layers whose length is at least $6L_{x0}$ along the $[0\bar{1}1]$ direction. The length of an N_{int}-interstitial cluster along the $\langle 011 \rangle$ direction is $N_{int}L_{x0}/2$. The orientation of the computational cells is chosen according to the symmetry of the interstitial chains. The bottom row shows E_{int}^{f} and E^{b}/N_{int} for the line defect–infinite interstitial chains along the $[1\bar{1}0]$ direction (Fig. 2). The size dependence of E_{int}^{f}'s shows that the interstitial clusters can trap interstitials to form more stable elongated structures.

N_{int}	I chain on the {311} plane[a]			I chain on the {100} plane[b]		
(eV)	E^{f}/N_{int}	E^{b}	E^{b}/N_{int}	E^{f}/N_{int}	E^{b}	E^{b}/N_{int}
2	4.7	−1.6	−0.8	4.9	−2.0	−1.0
3	3.7	0.6	0.2	3.4	1.5	0.5
4	3.4	2.0	0.5	3.3	2.4	0.6
5	3.0	4.5	0.9	2.9	5.0	1.0
6	2.8	6.6	1.1	2.8	6.6	1.1
∞	1.7		2.2	1.7		2.2

[a]Orientation of the computational cell: $[0\bar{1}1] \times [3\bar{2}\bar{2}] \times [311]$.
[b]Orientation of the computational cell: $[0\bar{1}1] \times [01\bar{1}] \times [100]$.

1.7 eV per interstitial and the corresponding bond-angle and bond-length distortions are $-15°$–$20°$ and -0.1–0.03 Å. We label the structure in Fig. 2(b) as an I chain on the {100} plane and that in Fig. 2(c) as an I chain on the {311} plane, based on the symmetry of the interstitial chains. These stable interstitial chains constitute basic building blocks of the {311} defects. Arranging interstitial chains side by side in the $\langle 233 \rangle$ direction results in the formation of even more stable extended defects lying on the {311} plane.

The small formation energy per interstitial (<2 eV) of the interstitial chain structures in Figs. 2(b) and 2(c) suggests that microscopic defects containing only a few interstitials may exist as stable structures as well. Interstitial clusters containing 2–6 interstitials are constructed by inserting finite-length interstitial chains into bulk Si. Table I gives the formation energies per interstitial (E_{int}^{f}) of finite-size interstitial clusters. Generally, E_{int}^{f} decreases as the size of interstitial defects increases, while the binding energy increases. This E_{int}^{f} dependence on the number of interstitials, i.e., the length of the interstitial chain, is consistent with experimental observation that the rodlike defects are extended along the $\langle 011 \rangle$ direction as long as 1μm.[11,12,28] The elongation of the {311} defects in the $\langle 011 \rangle$ direction is the consequence of the formation of the energetically favorable interstitial chain structures. This observation agrees with the energetic argument based on the minimum dangling-bond ratio of the $\langle 011 \rangle$ chain structures.

Table I shows that microscopic defects containing more than two interstitials are stable with respect to isolated interstitials.[32] A binding energy per interstitial can be interpreted as an average energy required to release interstitials from the interstitial clusters and the interstitial chains. The energy cost to evaporate interstitials increases as the size of the interstitial cluster grows: A smaller interstitial cluster would be dissolved at a lower annealing temperature or in a shorter period of time. Recent experiments reported boron
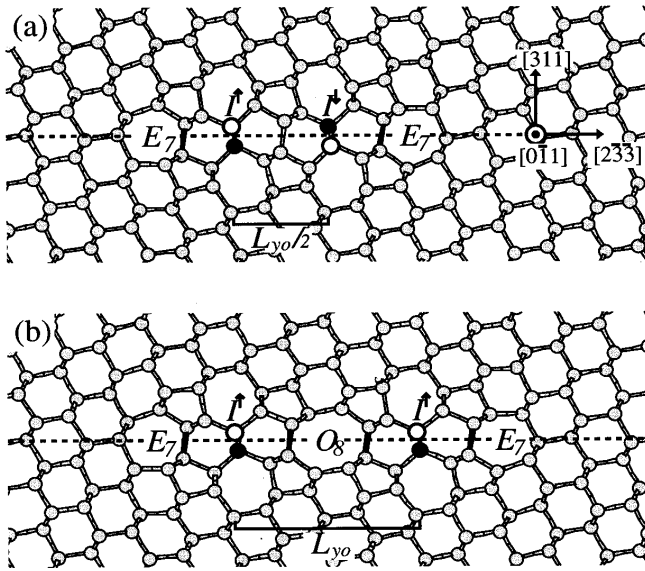
FIG. 3. Projections on the $\{0\bar{1}1\}$ plane of the rodlike $\{311\}$ defects containing two interstitial chains. The solid atoms (●) are deeper into the plane than the open-circled atoms (○) by $L_{x0}/2$. Interstitial chains are specified by the upper atoms with respect to the $\{311\}$ plane (dashed lines): (1) $I^{\uparrow}$, when the upper atoms are out of the $\{0\bar{1}1\}$ plane, and (2) $I^{\downarrow}$, when the upper atoms are into the $\{0\bar{1}1\}$ plane. The rodlike $\{311\}$ defects are believed to grow by adding interstitial chains along the $[2\bar{3}\bar{3}]$ direction. Total-energy calculations give the formation energy per interstitial at 1.5 eV for (a) and at 1.6 eV for (b). Seven-member rings (E_7's) form boundaries between the defects and the bulk Si, and they can be converted into six-member rings (E_6) by rotations of the solid bonds (heavy lines). In a similar way, an eight-member ring O_8 can be converted into either a seven-member ring (O_7) or a six-member ring (O_6). The stability of the E_7 and O_8 units depends on the arrangement of interstitial chains. A rotation of any solid bond of (a) increases the total energy. However, more stable structures can be obtained by rotations of the solid bonds in (b) as far as the transformation does not introduce adjacent five-member rings.

TED with a small activation energy (<2 eV) even when no macroscopic defects are detected.[8] The lack of extended defects in their samples was attributed to the low-energy ion-implantation condition. It is possible that few-interstitial clusters or interstitial chains, which are stable with respect to isolated interstitials, are generated during the low-energy ion implantation and contribute to the boron TED by providing interstitials during the thermal annealing.

IV. EXTENDED RODLIKE $\{311\}$ DEFECTS

A. Structure

Here we show that extended $\{311\}$ defects can be constructed by arranging the interstitial chains along the $\langle 233 \rangle$ direction. It has been observed that the rodlike defects elongated along the $\langle 011 \rangle$ direction grow thicker along the $\langle 233 \rangle$ direction, when there is a constant supply of interstitials.[12] Possible configurations consisting of two interstitial chains are shown in Fig. 3. Extended $\{311\}$ defects can be constructed by adding more interstitial chains along the

$[2\bar{3}\bar{3}]$ direction. As seen in Fig. 3, the $\{311\}$ habit plane of the defects is made of two orthogonal directions, the $\langle 011 \rangle$ and $\langle 233 \rangle$ directions. In forming defects extended along the $[2\bar{3}\bar{3}]$ direction, the arrangement of interstitial chains should satisfy following conditions: when two interstitial chains are separated by $L_{y0}/2$ as in Fig. 3(a), the pair include an $I^{\uparrow}$ and an $I^{\downarrow}$; when separated by L_{y0}, the pair consist of two identical interstitial chains, two $I^{\uparrow}$'s as in Fig. 3(b) or two $I^{\downarrow}$'s. Otherwise, dangling bonds are introduced and the corresponding distortions in bond angles become much larger than typical bond-angle distortions of $\pm 20°$ of the stable $\{311\}$ defects. Indeed, molecular-dynamics simulations at 600 K about 1 psec remove such configurations.

A different structure, an eight-member ring, is shown in Fig. 3(b). When two interstitial chains are separated by L_{y0} in the $[2\bar{3}\bar{3}]$ direction, there are three possible configurations: an eight-member ring (O_8), a seven-member ring (O_7), and a six-member ring (O_6). The three structures between two interstitial chains are related to each other by the same kind of planar rotations in Fig. 2. The eight-member ring in Fig. 3(b) can be converted into an O_7 or an O_6 unit by rotations of the solid bonds (heavy lines) on the $\{0\bar{1}1\}$ plane. An atomic model proposed by Takeda uses the eight-member ring as a basic unit in constructing the planar defects.[27,29,30] However, we consider three possibilities, the O_8, O_7, and O_6 units between two interstitial chains separated by L_{y0}. For all the structures we have studied, the six-member rings (O_6) between interstitial chains are found to be unstable with respect to the O_8 or O_7 units. A structure that forms a boundary between the defects and the bulk Si is denoted as E_7 according to the notation introduced by Kohyama and Takeda.[29,30] Similarly to the eight-member rings, the seven-member rings (E_7) can be converted into six-member rings (E_6) by planar rotations of the solid bonds in Fig. 3.

B. Energetics

The formation energies of *rodlike* $\{311\}$ defects containing few interstitial chains are listed in Table II. For example, the $E_7IIO_8IIE_7$ model structure has the following elements: I, interstitial chains; O_8, eight-member rings between the interstitial chains; and E_7, seven-member rings at the defect boundaries. Among possible combinations of the O and E units for the given arrangement of interstitial chains, configurations with a lower formation energy are listed in Table II. The rodlike defects become more stable with increasing number of interstitial chains (I units) in the $[2\bar{3}\bar{3}]$ direction as seen from the E_{int}^{f}'s of Table II: the formation energy decreases (i) when interstitial chains are added side by side in the $[2\bar{3}\bar{3}]$ direction with a distance $L_{y0}/2$ [Table II, (a) → (e)] and (ii) when interstitial chains are added in the $[2\bar{3}\bar{3}]$ direction in the presence of an O unit [Table II, (f) → (i)].

As seen in Table II, the eight-member rings (O_8) are stable when they are separated by a distance equal to or larger than L_{y0}. The formation energy of the $E_7IO_8IE_7$ model structure is lowered by 0.1 eV by transformation of the O_8 unit to a seven-member ring (O_7). On the other hand, the eight-member ring of $E_7IIO_8IIE_7$ model is stable with respect to the $E_7IIO_7IIE_7$ structure. Similarly, we observe that the seven-member ring at a defect boundary is stable if there are more than two I units inserted between E_7 and the

TABLE II. Formation energy of extended $\{311\}$ defects consisting of interstitial chains. The computational cell is $3L_{x0} \times 6L_{y0} \times 2L_{z0}$ containing three unit cells in the $[0\bar{1}1]$ direction for all listed model structures. The ratio of the I unit to the extent of defects is given in percentage, e.g., $3/6 = 50\%$ for the $E_7IIO_8IE_7$ structure. The energy release ΔE_I is defined in Eq. (3) upon adding an interstitial chain (I) to the rodlike defect X. Y denotes a defect structure constructed by adding an I with a distance of either $L_{y0}/2$ or L_{y0} from the boundary interstitial chain of the defect X.

Model structure	N_{int} (% of I units) (per unit cell[a])	E_{int}^f (eV)	ΔE_I: $X + I \rightarrow Y$
(a) E_7IE_7[b]	2 (67)	1.8[c]	1.2: (a)$+I\rightarrow$ (b)
			0.9: (a)$+I\rightarrow$ (f)
(b) E_7IIE_7	4 (50)	1.5	1.6: (b)$+I\rightarrow$ (c)
			1.0: (b)$+I\rightarrow$ (g)
(c) E_7IIIE_7	6 (60)	1.3	1.2: (c)$+I\rightarrow$ (d)
			0.6: (c)$+I\rightarrow$ (h)
(d) E_7IIIIE_7	8 (67)	1.3	1.0: (d)$+I\rightarrow$ (e)
(e) $E_7IIIIIE_7$	10 (71)	1.3	
(f) $E_7IO_7IE_7$ or $E_7IO_8IE_6$	4 (40)	1.6	1.3: (f)$+I\rightarrow$ (g)
(g) $E_7IIO_7IE_7$ or $E_7IIO_8IE_6$	6 (50)	1.4	1.1: (g)$+I\rightarrow$ (h)
			1.3: (g)$+I\rightarrow$ (i)
(h) $E_7IIIO_7IE_7$ or $E_7IIIO_8IE_6$	8 (57)	1.3	
(i) $E_7IIO_8IIE_7$	8 (57)	1.3	

[a]Unit cell: $L_{x0} \times 6L_{y0} \times 2L_{z0}$.
[b]Identical to the I chain on the $\{311\}$ plane in Fig. 2(c).
[c]$E_{int}^f = 1.7$ eV for a unit cell $L_{x0} \times 3L_{y0} \times 2L_{z0}$.

closest O or E unit. For example, the total energy increases when the seven-member rings (E_7's) are converted into six-member rings for the E_7IIE_7 and $E_7IIO_8IIE_7$ models.

We define an energy release ΔE_I, when an interstitial chain is added to a rodlike defect X containing N_{int} interstitials per L_{x0}, as
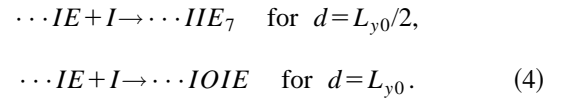
$$\Delta E_I = (N_{int}E_{int}^f[X] + 2E_{int}^f[E_7IE_7]) - (N_{int} + 2)E_{int}^f[X+I].$$ (3)

The formation energy $E_{int}^f[E_7IE_7] = 1.8$ per interstitial is used as the formation energy of an isolated interstitial chain, which contains two interstitials per unit length L_{x0}. The energy release ΔE_I for the $E_7IIO_8IE_7$ structure to capture an interstitial chain and become the $E_7IIO_8IIE_7$ structure is 1.6 eV per unit length (L_{x0}). On the other hand, $\Delta E_I = 1.0$ eV for the E_7IIIE_7 structure to become the E_7IIIIE_7 structure. The larger ΔE_I for the $E_7IIO_8IE_7$ structure indicates that the $E_7IIO_8IE_7$ structure provides a more efficient sink of interstitials than the E_7IIIE_7 structure, which contains the same number of interstitials per unit cell. The ΔE_I's for the E_7IIE_7 structure suggest that the interstitials can be evaporated with a smaller energy cost from the $E_7IIO_8IE_7$ structure than from the E_7IIIE_7 structure.

Growth mechanisms of the $\{311\}$ defects are suggested by both the E_{int}^f at different interstitial concentrations and the energy release ΔE_I, when an interstitial chain is added to an existing $\{311\}$ defect. Previously we showed that an interstitial chain can exist as a stable structure against isolated interstitials with $E_{int}^f < 2.2$ eV, which is smaller than that of isolated interstitials. The interstitial chain can provide a sink of interstitials to capture interstitial chains along the $[2\bar{3}\bar{3}]$

direction. Reactions that release a larger energy to capture an interstitial chain are more likely to happen during the growth process.

We express the capturing of an interstitial chain by a rodlike $\{311\}$ defect symbolically, as

$$\cdots IE + I \rightarrow \cdots IIE_7 \quad \text{for} \quad d = L_{y0}/2,$$

$$\cdots IE + I \rightarrow \cdots IOIE \quad \text{for} \quad d = L_{y0}. \quad (4)$$

Here d is the distance of the additional interstitial chain from the boundary interstitial chain. Table II shows that the energy release by the addition of an interstitial chain is similar for either $d = L_{y0}/2$ or $d = L_{y0}$, which suggests that the interstitial-chain capturing mechanisms in Eq. (4) are equally likely to happen. In other words, an interstitial chain can be added next to the boundary interstitial chain with a distance either $L_{y0}/2$ or L_{y0}. Consequently, the O units would be randomly introduced and the $\{311\}$ defects would have no particular periodic arrangement of the interstitial chains. In fact, experiments observe no particular periodicity of the $\{311\}$ defects in the $\langle 233 \rangle$ direction,[28] while the periodicity in the $\langle 011 \rangle$ direction is identified to be L_{x0}, which results from the interstitial chain structure.

We denote the "interstitial density" D_{int} to be a ratio of the number of interstitial *chains* to the total number of units in the defects:

$$D_{int} \equiv \frac{N[I]}{N[I] + N[O] + N[E]}. \quad (5)$$

We obtain the optimal ratio of the interstitial chains of 67% for the $\{311\}$ defects based on the following results. (i) The formation energy for the extended defects (3)–(5) in Table II

is same with differences less than 0.1 eV. This formation energy $E_{int}^f = 1.3$ eV is smaller than $E_{int}^f = 1.4$ eV of a planar defect, i.e., an infinite sequence of the interstitial chains in the $[23\bar{3}]$ direction ($\cdots IIII \cdots \equiv /I/$). (ii) The planar defect consisting of sequences of the IIO_8 structure, the $\cdots IIO_8 IIO_8 \cdots \equiv /IIO_8/$ model, is found to be very stable with the smallest $E_{int}^f = 1.2$ eV among the model structures we have investigated. This interstitial density (67%) is in good agreement with the observed ratio of I units, 62% from high resolution transmission electron microscopy (HRTEM) images.[27]

V. PROPAGATION OF INTERSTITIAL CHAINS

So far we have discussed the energetics of classes of defects, from the interstitial clusters to the extended {311} defects, solely in terms of the formation energies. It has been shown that the interstitial clusters can bind interstitials and become elongated interstitial chains along the ⟨011⟩ direction. The interstitial chains in turn grow to the extended {311} defects by capturing interstitials along the ⟨233⟩ direction. We propose that successive planar rotations, which introduce eight-member rings between interstitial chains separated by L_{y0}, can also displace interstitial chains. By successive rotations of atoms connected by solid bonds in Fig. 4, an interstitial chain characterized by the {311} habit plane is displaced by $\Delta = 2a/\sqrt{2}$ along the arrow (the $[0\bar{1}\bar{1}]$ direction), perpendicular to the $[0\bar{1}1]$ chain direction. The planar rotations connect two interstitial chain structures with the same $E_{int}^f = 1.7$ eV: the I chain on the {311} plane, [Figs. 4(a)–4(d)] and the I chain on the {100} plane [Figs. 4(b) and 4(e)].

This kind of coordinated atomic motion was introduced by Pandey as a diffusion mechanism of Si atoms in a thermal equilibrium without introducing point defects.[33] He suggested that successive rotations of nearest-neighboring atoms in the $\{0\bar{1}1\}$ plane and the {011} plane result in exchanges of atoms and eventually displacements of Si atoms. The interstitial chain configurations shown in Fig. 4 are related to each other by $\phi \sim 70°$ rotation of the pair atoms (solid circles) in the $\{0\bar{1}1\}$ plane.

For E^f, a formation energy of the interstitial chain, E_b, an energy barrier for the propagation, and S, an entropy involved with the propagation, the probability for an interstitial chain to propagate is proportional to $\exp\{-(E^f + E_b - TS)/k_B T\}$. The propagation mechanism of the interstitial chains via planar rotations has such desirable features: (i) no dangling bond is introduced during the transformation due to atomic relaxations and thus a small energy barrier is expected and (ii) the entropy involved with the rotation may be high because of the large extent of atomic relaxations and many possible paths.

An energy barrier for the transformation from the structure of Figs. 4(a) and 4(b) is estimated in two ways. First, an energy barrier for the rotation is estimated by calculating total energies of saddle points and comparing the total energies with those of the interstitial chain structures. The calculations are performed at a fixed computation cell of $4L_{x0} \times 3L_{y0} \times 2L_{z0}$. This computational cell contains four solid bonds in the $\{0\bar{1}1\}$ plane, which are not shown in Fig. 4(a). The saddle-point configurations are initially given by
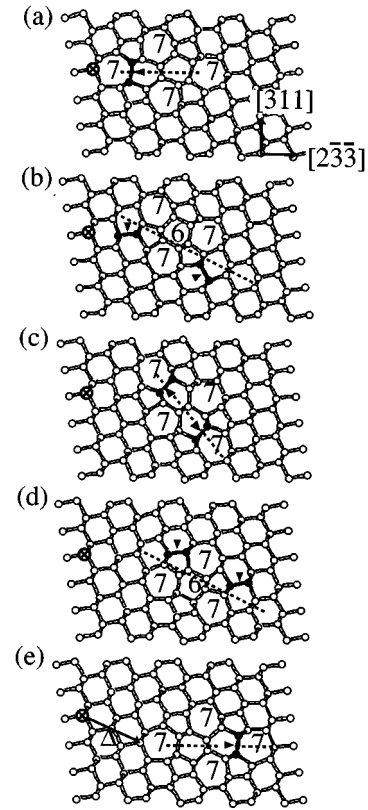

FIG. 4. By succesive rotations of solid atoms connected by solid bonds, an interstitial chain on the {311} habit plane is displaced by $\Delta = 2a/\sqrt{2}$ along the perpendicular direction of the interstitial chain (arrow). The ⊗ denotes a reference atom. Intermediate structures are characterized by the habit planes: the {100} plane for (b) and (d) and the {311} plane for (c), indicated by dashed lines. The formation energy per interstitial of the illustrated structures is 1.7 eV for a fixed computational cell. The dimension of the cell is $4L_{x0} \times 3L_{y0} \times 2L_{z0}$.

simultaneously rotating the atoms connected by the solid bonds by $\phi = 15°$, 30°, and 45° on the $\{0\bar{1}1\}$ plane. The bond length of the two atoms is chosen at the average value of the bond lengths of two structures in Figs. 4(a) and 4(b). Then structural relaxations of the initial configurations are performed by allowing all atoms to move, except for the two rotated atoms. The rotated atoms are fixed at the intermediate positions. The calculated energy barrier is 1.7 eV per bond. When the similar rotation of two atoms is performed in the bulk Si without any interstitial, the energy barrier is about 2.7 eV per bond.

Alternatively, the energy barrier is estimated by rotating one bond at a time among four solid bonds in a computational cell, which are underneath the solid bond in Fig. 4(a) in the $[0\bar{1}1]$ direction. For rotations of one to three bonds, the total energy increases by 1.2 ± 0.1 eV in comparison to those of the interstitial chains in Figs. 4(a) and 4(b). The corresponding increase in the formation energies is less than 0.2 eV per interstitial. No dangling bond is introduced by these planar rotations and the intermediate structures have bond-angle distortions of $\pm 22°$, slightly larger than the $-15°$–$20°$ bond-angle distortions of the interstitial chain configurations in Figs. 4(a) and 4(b).
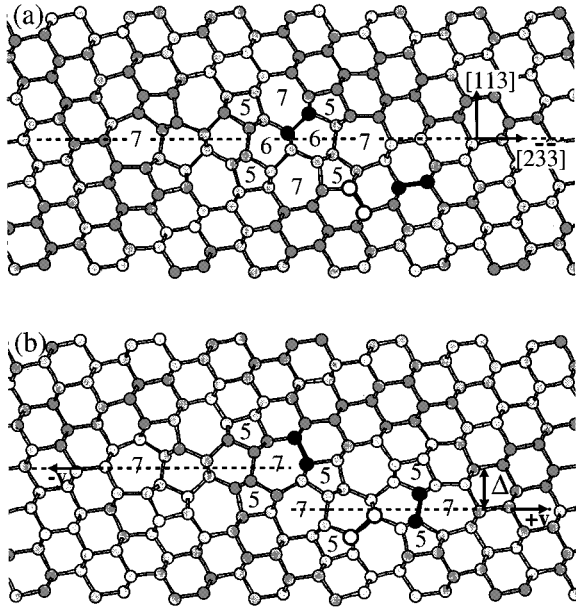
The energy barriers estimated by two different paths sug-

FIG. 5. By rotations of three solid bonds, a rodlike {311} defect containing two I chains on the {311} plane (a) is transformed to a step configuration with a height of $\Delta = a/\sqrt{11}$ along the [311] direction (b). The solid atoms are deeper into the plane by $L_{x0}/2$ than the open-circled atoms. The difference of the total energies per unit cell of the two structures, which contains 528 bulk Si atoms, is less than 0.1 eV and the corresponding ΔE_{int}^f is less than 0.05 eV. Intermediate states after rotations of one or two solid bonds have the same E_{int}^f.

gest that many possible combinations of the planar rotations, which has an energy barrier less than 2 eV per bond, can lead to the displacements of interstitial chains. The growth of the {311} defects along the $\langle 233 \rangle$ direction during thermal annealing[10] can be explained by the coalescence of interstitial chains that propagate via the planar rotations. The same mechanism may be responsible for the unfaulting of the {311} defects, which relates the {311} defects with the perfect dislocation loops at high temperatures $(> 1000$ K).[11]

VI. STEP STRUCTURES AND V-SHAPED BENDS

We now show that step structures and V-shaped bends found in the extended {311} defects can be constructed by combination of rotations of nearest-neighboring atoms on the $\{0\bar{1}1\}$ plane together with the interstitial chain structures. Rotations of three solid bonds in Fig. 5(a) result in a displacement of the right interstitial chain. The formation energy of the structures before and after the transformation is the same at $E_{int}^f = 1.5$ eV. The structure in Fig. 5(b) is similar to the core model of the atomic steps observed in HRTEM images.[28] The addition of interstitial chains to this defect structure along the $\pm$ **y** direction (the $[2\bar{3}3]$ direction) leads to the formation of a defect structure containing an atomic step. The two {311} habit planes shown as dashed lines are separated by a step height of $\Delta = a/\sqrt{11}$ along the {311} direction, which agrees with that predicted in Ref. 24.

It has been observed that the {311} defects change habit planes, for example, between the {311} and $\{3\bar{1}1\}$ planes. The atomic configuration around the bend where the habit

planes change can be identified as the I chain in the {100} plane in Fig. 2(b). We show in Fig. 6 that the interstitial chains can be added to an I-chain {100} plane to form a V-shaped defect. The initial configuration, when two interstitial chains are added, is chosen so as to avoid the generation of adjacent five-member rings by bond rotations on the $\{0\bar{1}1\}$ plane. The lowest-energy configuration of the bend structure is found to have seven-member rings at the edges (E_7): By transformation of the six-member rings to E_7's, the total energy is lowered by 3.8 eV per cell,[34] corresponding to $\Delta E_{int}^f = -0.2$ eV. The bond-angle distortion ranges between $-17°$ and $26°$ and the bond-length distortion between -0.1 Å and 0.02 Å. The formation energy, 1.3 eV per interstitial, is comparable to that of the $E_7 I I I E_7$ model structure at the same interstitial concentration of 6 per unit length, $L_{x0} = a/\sqrt{2}$. The defect can grow on both habit planes, the {311} and $\{3\bar{1}1\}$ planes, by capturing interstitials or interstitial chains. The stability of the E_7's suggests that the additional interstitial chains are to be separated by L_{y0}. In other words, for the center interstitial chain $\tilde{I}$, the V-shaped bend structure is likely to have an interstitial arrangement as $\cdots I O_8 I \tilde{I} I O_8 \cdots$.

VII. PLANAR {311} DEFECTS

Extended {311} defects as wide as 100 nm along the $\langle 233 \rangle$ direction are studied by approximating them as planar defects that are periodic in both the $\langle 011 \rangle$ and the $\langle 233 \rangle$ directions.[35] Formation energies of planar defects, constructed by combinations of interstitial chains (I) and eight-member rings (O_8) along the $[2\bar{3}3]$ direction, are listed in Table III. As introduced by Kohyama and Takeda,[29] the periodicity of a planar defect along the $[2\bar{3}3]$ direction is specified by an arrangement of I's and O's within a unit cell, which is denoted by //. For example, the $/IIO_8/$ model contains two I units separated by a distance of $L_{y0}/2$ in the $[2\bar{3}3]$ direction and one O_8 unit within a unit cell. The periodicity of the $/IIO_8/$ model along the $[2\bar{3}3]$ direction is $3(L_{y0}/2)$, where $L_{y0}/2$ is the average width of each unit and the factor 3 is the total number of units within a unit cell.

The formation energy per interstitial of the planar {311} defects is significantly smaller than that of isolated interstitials and comparable to that of the extended {311} defects with finite widths along the $[2\bar{3}3]$ direction (Table II). The stability of the planar defects against isolated interstitials indicates that the {311} defects can grow indefinitely as long as the interstitials are supplied, e.g., during the ion implantation process. Among the model structures we have investigated, the $/IIO_8/$ model is the lowest in the formation energy per interstitial ($E_{int}^f = 1.2$ eV). The density of the I units of the $/IIO_8/$ planar defect is 67%, corresponding to the interstitial concentration of $5 \times 10^{14}/\text{cm}^2 = 4/[L_{x0} \times 3(L_{y0}/2)]$.

The model structure with adjacent O_8 units along the $[2\bar{3}3]$ direction is energetically least favorable at the same interstitial concentration in comparing the $/IIO_8/$, $/IIIO_8 IO_8/$, and $/IIIIO_8 O_8/$ models. In fact, segments including two adjacent eight-member rings, $\cdots O_8 O_8 \cdots$, have not been identified as local structures of the extended {311} defects.[27,28] When a planar rotation is applied on the common bond shared by the neighboring eight-member rings
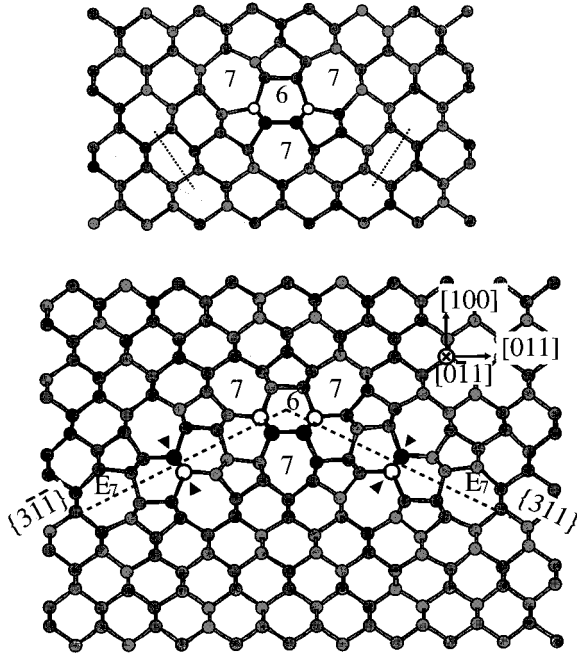
FIG. 6. Bend configuration of the {311} defects (bottom) obtained by the addition of two interstitial chains to an I chain on the {100} plane (top). Insertion of interstitial chains results in breaking of bonds (dotted lines). The bottom structure contains six interstitials per unit length of L_{x0}: two interstitials associated with the I chain on the {100} plane and four additional atoms indicated by arrows. A row of the center six-member rings along the $[0\bar{1}1]$ direction forms a boundary of the defects, which have the {311} and {$3\bar{1}1$} habit planes (dashed lines). This V-shaped defect has a mirror symmetry with respect to the center of the six-member rings. The formation energies per interstitial are 1.7 eV (top) and 1.3 eV (bottom). Further growth of the defect can occur by the addition of interstitial chains on both habit planes.

of the /$IIIIO_8O_8$/ model, E_{int}^f is lowered by 0.2 eV. The stability of the eight-member rings of each structure is studied by applying planar rotations of the atoms that form boundaries between the eight-member rings and six-member rings along the $[2\bar{3}\bar{3}]$ direction. The last column of Table III shows that the O_8's are stable when their separation is equal to or larger than L_{y0}, consistently with the result of the finite-width {311} defects.

The difference of the E_{int}^f's of the /IIO_8/ and /$IIIO_8IO_8$/ models implies that the stability of the planar defects is determined not only by the density of interstitial chains but also by the arrangement of interstitial chains. Planar defects containing isolated interstitial chains between O units ($\cdots OIO \cdots$) have higher formation energies than those without them at the same interstitial concentration. The energy gain by the transformation of one of the eight-member rings to a seven-member ring is insufficient to change the relative stabilities of the planar defects. Based on the E_{int}^f of the planar defects listed in Table III, we expect that the /$IIIO_8IIO_8$/ and /$IIIO_8$/ planar defects to have comparable E_{int}^f to the most stable planar defect, the /IIO_8/ model.

The formation energy of the planar defects we have discussed is obtained without allowing relaxation of the supercells. A supercell relaxation would have generated the dis-

TABLE III. Formation energies per interstitial (E_{int}^f) of planar {311} defects consisting of interstitial chains and eight-member rings. The periodicity of the structures along the $[2\bar{3}\bar{3}]$ direction is denoted by //. The number of interstitials and the formation energy are given per unit area, $L_{x0} \times 3L_{y0}$, in order to compare structures with different periodicities along the $[2\bar{3}\bar{3}]$ direction. The same computational cell is used for the total-energy calculations of all the listed structures with two choices for the length of the cell in the [311] direction, $2L_{z0}$ and $3L_{z0}$. The last column shows the stability of the eight-member rings and the most stable planar defects that can be obtained by rotations of atoms on {$0\bar{1}1$}.

Model structure	N_{int}[a]	$E_{int}^f (eV)$		Stability of O_8 units
		$2L_{z0}$	$3L_{z0}$	
/I/	12	1.35	1.27	
/IO_8/	6	1.68	1.59	unstable, /$IO_7IO_7IO_8$/
/IIO_8/	8	1.23	1.16	stable
/$IIIO_8IO_8$/	8	1.35	1.26	unstable, /$IIIO_7IO_8$/
/$IIIIIO_8$/	10	1.24	1.18	stable
/$IIIIO_8O_8$/	8	1.48		unstable, /$IIIIO_7O_7$/

[a]Per unit area: $L_{x0} \times 3L_{y0}$.

placement vector (Burger vector) around the core of the {311} defects identified by TEM observations.[13,28] However, we anticipate that the *relative stability* is correctly described by the fixed cell calculations. The critical dimension to obtain the converged formation energy for the planar defects is L_z, the length of the supercell in the [311] direction. We obtain the formation energies of the planar defects at $L_z = 3L_{z0}$ and the formation energies are also listed in Table III. The formation energy is lowered by 0.08 eV on average for all the planar defects. The relative stability of the planar defects is the same for $L_z = 2L_{z0}$ and $3L_{z0}$.

In Fig. 7 we show the formation energy of the defects that are infinite along the $[2\bar{3}\bar{3}]$ direction and finite ($L_D = n_D L_{x0}$) along the $[0\bar{1}1]$ direction. The elongation direction of the {311} defects is always along the $\langle 011 \rangle$ direction. However, we study the hypothetical defect structures with lengths (L_D) shorter than the width in the $[2\bar{3}\bar{3}]$ direction to compare with the planar defects. Since the infinite limits of these defects ($L_D \propto \infty$) are planar defects, we can compare the formation energy of the planar defects in Table III with $E_{int}^f[\infty]$, which can be extracted from the finite-length-defect calculations.

The defect structures in Fig. 7 are constructed by inserting a finite-length planar defect between bulk layers. The defects become either the /I/ or /IO_8/ model structure at the infinite limits. The formation energy increase linearly to the length along the $[0\bar{1}1]$ direction:

$$E^f = E_{edge}^f + N_{int}E_{int}^f[\infty]. \qquad (6)$$

Then the E_{int}^f of the defects with respect to the length is written as

$$E_{int}^f = E_{int}^f[\infty] + E_{edge}^f/N_{int} \propto 1/L_D. \qquad (7)$$

The slopes $E_{int}^f[\infty]$ of two kinds of defects is the formation energy per interstitial at the infinite limits, i.e., $N_{int} \propto L_D \rightarrow \infty$. The slopes obtained from linear fittings are in good agreement with the E_{int}^f's in Table III: 1.4 eV and 1.7
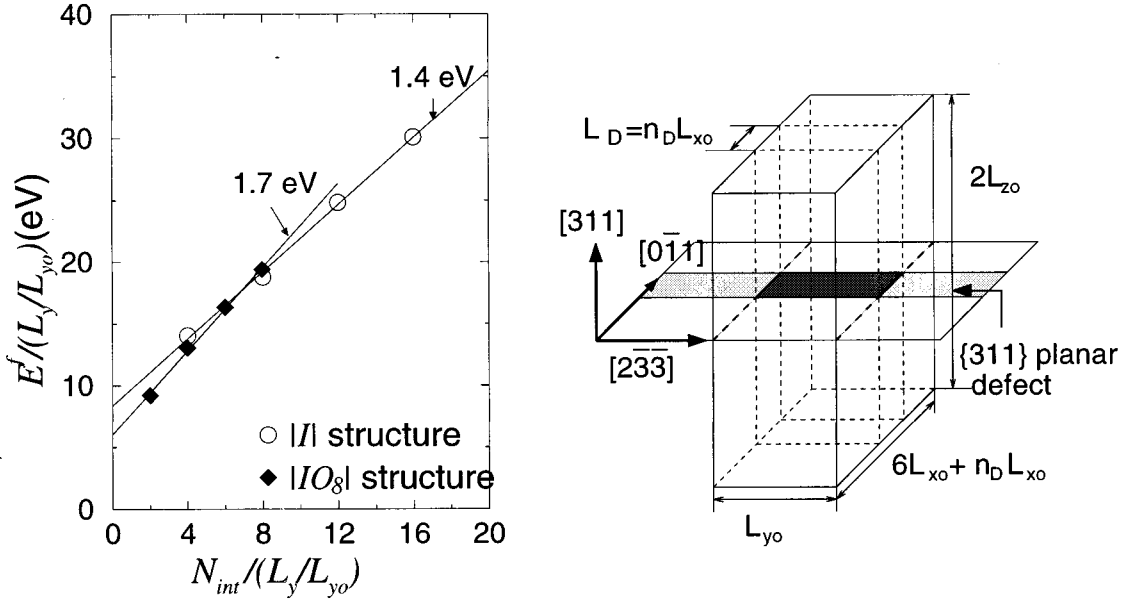
FIG. 7. Formation energy (E^f) per unit width (L_{y0}) with respect to the number of interstitials per unit width (left); a schematic diagram to show how the computational cell is constructed (right). A slab with a finite length of $n_D L_{x0}$, for an integer $n_D = 1-4$, contains defect structures based on the $/IO_8/$ and $/I/$ models. The slab is sandwiched between Si bulk layers along the $[0\bar{1}1]$ direction with a fixed total length of $6L_{x0}$. A common width along the $[2\bar{3}\bar{3}]$ direction is chosen at L_{y0}. The number of interstitials per unit width (L_{y0}) is proportional to the length of the defects: $N_{int} = 4n_D$ for the defects based on the $/I/$ model and $N_{int} = 2n_D$ for those based on the $/IO_8/$ model. The formation energy is fitted by Eq. (6). For the defects based on the $/I/$ model, the values of E_{edge}^f and $E_{int}^f[\infty]$ are 8.4 and 1.4 eV, respectively; $E_{edge}^f = 6.1$ eV and $E_{int}^f[\infty] = 1.7$ eV for the defects derived from the $/IO_8/$ model. The formation energy per interstitial decreases as the length increases as in Eq. (7). At $N_{int} \to \infty$, the E_{int}^f's converge to those of the planar defects: 1.4 eV for the $/I/$ model and 1.7 eV for the $/IO_8/$ model.

eV for the $/I/$ model and $/IO_8/$ model, respectively. This result confirms that the $/I/$ model is more stable than the $/IO_8/$ model.

Finally, the ability of the {311} defects to capture or release interstitials is studied by calculating an energy required to add an interstitial to the bulk Si in the presence of the planar defects (Fig. 8). An interstitial is added at the hexagonal site at a distance of h from the {311} habit plane. The eight-member rings of the $/IO_8/$ planar defect can provide efficient sinks of interstitials; the extra energy to add an interstitial to the $/IO_8/$ planar defect decreases with decreasing h: 3.2 eV at 16.5 Å and 1.5 eV at 10.1 Å. When the interstitial is added right above the eight-member ring (3.8 Å from the habit plane), about 0.1 eV energy is released. On the other hand, an additional interstitial is not bounded by the $/IIO_8/$ planar defect. The energy required to add an interstitial is 4.7–5.1 eV. This energy is comparable to the formation energy of an isolated interstitial at the hexagonal sites and larger than that of the $\langle 110 \rangle$ interstitialcy. These results support the calculations showing that the saturation of interstitials is achieved at the I density about 67% in the $/IIO_8/$ structure (Table III).

VIII. CONCLUSION

We have shown that interstitial chain structures elongated along the $\langle 011 \rangle$ direction constitute the basic building blocks of the extended {311} defects. This interstitial chain configuration is favored due to the minimum ratio of dangling bonds per interstitial and small distortions in bond angles and bond
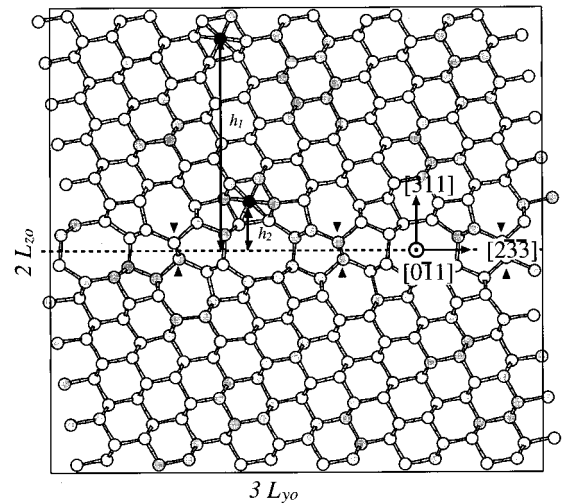

FIG. 8. Initial configurations to obtain the extra energy required to add *one* interstitial to the bulk system in the presence of a planar defect. The additional interstitial is located at a hexagonal site with a distance h measured from the {311} plane on which the center of interstitial chains lie (the dashed line). Two cases with $h_1 = 16.5$ Å and $h_2 = 3.8$ Å are illustrated at the same time. The computational cell is $6L_{x0} \times 3L_{y0} \times 2L_{z0}$. The distance of interstitials in the neighboring cells, i.e., the distances between images related by periodic boundary conditions, is larger than the distance of the additional interstitial to the habit plane of the planar defect. The interstitials associated with the interstitial chains of the $/IO_8/$ model structure are indicated by arrows.

lengths. Even finite-size interstitial chains, as small as two-interstitial clusters, are found to be stable against isolated interstitials. A growth mechanism of the {311} defects can be speculated from the dependence of the E_{int}^f's on the dimensions of the defects and the interstitial concentrations. The growth of the {311} defects would occur first by (i) elongation of interstitial chains along the $\langle 011 \rangle$ direction and (ii) the widening of the defects follows by capturing interstitial chains alongside the $\langle 233 \rangle$ direction. We present an efficient mechanism, rotations of atoms on the {011} plane, which can lead to propagation of interstitial chains. The planar rotation, together with the interstitial chain structures, can be applied to explain growth process of the {311} defects and related structures such as the V-shape bend structure and atomic steps. We observed that the most stable arrangement of interstitial chains of the extended {311} defects is $\cdots IIO_8IIO_8\cdots$ and the optimal density of interstitial chains is 67%, which is in good agreement with the experimental value of 62%.

[*]Present address: National Renewable Energy Laboratory, Golden, CO 80401.

[1]P. M. Fahey, P. B. Griddin, and J. D. Plummer, Rev. Mod. Phys. **61**, 289 (1989), and references therein.

[2]A. E. Michel, W. Rausch, P. A. Ronsheim, and R. H. Kastl, Appl. Phys. Lett. **50**, 416 (1987).

[3]P. A. Stolk, H.-J. Gossmann, D. J. Eaglesham, and J. M. Poate, Appl. Phys. Lett. **66**, 568 (1995).

[4]A. Bourret, in *Microscopy of Semiconducting Materials*, Proceedings of the IOP Conf. Series No. 87, edited by A. G. Cullis and P. D. Augustus (Institute of Physics and Physical Society, London, 1987), p. 39.

[5]R. Car, P. J. Kelly, A. Oshiyama, and S. T. Pantelides, Phys. Rev. Lett. **54**, 360 (1984).

[6]C. S. Nichols, C. G. Van de Walle, and S. T. Pantelides, Phys. Rev. B **40**, 5484 (1989).

[7]A. E. Michel, Nucl. Instrum. Methods Phys. Res. Sect. B **37**, 379 (1989).

[8]L. H. Zhang, K. S. Jones, P. H. Chi, and D. S. Simons, Appl. Phy. Lett. **67**, 2025 (1995).

[9]D. J. Eaglesham, P. A. Stolk, H.-J. Gossmann, and J. M. Poate, Appl. Phys. Lett. **65**, 2305 (1994).

[10]P. A. Stolk, H.-J. Gossmann, D. J. Eaglesham, and J. M. Poate, Nucl. Instrum. Methods Phys. Sect. B **96**, 187 (1995).

[11]L. G. Salisbury and M. H. Loretto, Philos. Mag. A **39**, 317 (1979).

[12]C. A. Ferreira Lima and A. Howie, Philos. Mag. **34**, 1057 (1976).

[13]M. D. Matthews and S. J. Ashby, Philos. Mag. **27**, 1313 (1973).

[14]F. Mauri, G. Galli, and R. Car, Phys. Rev. B **47**, 9973 (1993); P. Ordejón, D. Drabold, M. Grunbach, and R. Martin, *ibid.* **48**, 14 646 (1993); F. Mauri and G. Galli, *ibid.* **50**, 4316 (1994); P. Ordejón, D. Drabold, R. Martin, and M. Grunbach, *ibid.* **51**, 1456 (1995); J. Kim, F. Mauri, and G. Galli, *ibid.* **52**, 1640 (1995).

[15]I. Kwon, R. Biswas, C. Z. Wang, K. M. Ho, and C. M. Soukoulis, Phys. Rev. B **49**, 7242 (1994).

[16]M. Menon and K. R. Subbaswamy, Phys. Rev. B **50**, 11 577 (1994).

[17]R. Car, P. J. Kelly, A. Oshiyama, and S. T. Pantelides, Phys. Rev. Lett. **52**, 1814 (1984).

[18]Y. Bar-Yam and J. D. Joannopoulos, Phys. Rev. B **30**, 1844 (1984).

[19]D. J. Chadi, Phys. Rev. B **46**, 9400 (1992).

[20]P. E. Blöchl, E. Smargiassi, R. Car, D. B. Laks, W. Andreoni, and S. T. Pantelides, Phys. Rev. Lett. **70**, 2435 (1993).

[21]J. Kim, Ph.D. dissertation, The Ohio State University, 1996.

[22]We considered $p(2\times 1)$ symmetric, $p(2\times 1)$ asymmetric, and $c(4\times 2)$ dimerization of Si(100) surfaces. The surface energy is lowest for the $c(4\times 2)$ reconstruction and highest for the $p(2\times 1)$ symmetric reconstruction. These results are consistent with the recent *converged* LDA calculations by Ramstad *et al.* [Phys. Rev. B **51**, 14 504 (1995)].

[23]R. W. Nunes, J. Bennetto, and D. Vanderbilt, Phys. Rev. Lett. **77**, 1516 (1996).

[24]Q. Li and R. Biswas, Phys. Rev. B **50**, 18 090 (1994); **52**, 10 705 (1995).

[25]A. Canning, G. Galli, F. Mauri, A. De Vita, and R. Car, Comput. Phys. Commun. **94**, 89 (1996).

[26]T. Y. Tan, Philos. Mag. A **44**, 101 (1981).

[27]S. Takeda, Jpn. J. Appl. Phys. **30**, L639 (1991).

[28]S. Takeda, M. Kohyama, and K. Ibe, Philos. Mag. A **70**, 287 (1994).

[29]M. Kohyama and S. Takeda, Phys. Rev. B **46**, 12 305 (1992). The symbols for the structural units (I, O, and E) are adapted to describe the extended {311} defects.

[30]M. Kohyama and S. Takeda, Phys. Rev. B **51**, 13 111 (1995).

[31]The same $E_{int}^f = 1.7$ eV is obtained from a calculation using a computational cell oriented as $[0\bar{1}1]\times[011]\times[100]$.

[32]We note that the initial atomic configuration of the finite-size interstitial clusters is constructed based on the infinite interstitial chains in Fig. 2 and the *local energy minima* of the atomic configurations are obtained by the steepest-decent methods. For the two-interstitial clusters with a negative binding energy, we perform high-temperature MD simulations at 600–900 K for 1–2 ps and then search for low-energy atomic configurations by simulated annealing procedure, while slowly lowering the temperature of the systems. For the given simulation time and temperatures, we do not observe any breakup of the interstitial clusters and, furthermore, we find a low-energy configuration of the two-interstitial clusters, with a formation energy, 3.5 eV per interstitial.

[33]K. C. Pandey, Phys. Rev. Lett. **57**, 2287 (1986).

[34]The orientation and size of the computational cell is $3a/\sqrt{2}[0\bar{1}1]\times 12a/\sqrt{2}[011]\times 7a[100]$ for the lattice constant

a. The cell contains 1008 bulk Si atoms.

[35] Experimentally, a displacement vector of the perfect crystals around the core of the {311} defects was identified as $0.14a/\sqrt{11}$ along the $[2\bar{3}\bar{3}]$ direction and $0.64a/\sqrt{11}$ along the [311] direction. Our structural optimizations are performed by fixed cell calculations without a rigid body translation. All the atoms in the computational cells are allowed to relax.